Hindawi
International Journal of Antennas and Propagation
Volume 2021, Article ID 2118059, 12 pages
https://doi.org/10.1155/2021/2118059

Research Article

Compact Four-Port Dual-Sense Circularly Polarized Stack-Up Patch Antenna for UHF/MW-RFID MIMO System

Enze Zhang and Jinghui Qiu

School of Electronics and Information Engineering, Harbin Institute of Technology, Harbin 150001, China

Correspondence should be addressed to Enze Zhang; zez1992@foxmail.com

Received 24 June 2021; Revised 6 August 2021; Accepted 21 August 2021; Published 30 August 2021

Academic Editor: Giovanni Andrea Casula

A four-port dual-band dual circularly polarized (CP) stack-up patch antenna is introduced for multiple-input-multiple-output (MIMO) RFID application. The proposed antenna adopts two FR 4 substrates and one Rogers Ro4350b substrates. Two pairs of isolated ports work at FCC UHF/MW-RFID bands (0.902–0.928 and 2.4–2.485 GHz) with port isolations of 20 dB and 25 dB, respectively. Four inverted-F radiating elements fed with a 90° phase-delay feeding network realize the CP radiation at the FCC UHF-RFID band (0.902–0.928 GHz). The corner-truncated square slot and patch are implemented to obtain CP modes at the MW-RFID band. The relative impedance bandwidths in the FCC UHF and MW band are 10.9% and 9.4%, respectively, with peak gains of 4.1 and 7.2 dBic. The antenna's MIMO performance of envelope correlation coefficient (ECC) is lower than 0.01, and diversity gain (DG) is close to 10 dB. Thanks to the stack-up configuration, the dual-band RFID antenna realizes good antenna performance with a compact size of $0.6 \times 0.6 \times 0.07\,\lambda^3$.

1. Introduction

Recently, the radio-frequency identification (RFID) technique is a widespread research tendency for some fields, such as biomedicine, traffic, and logistics, because of its practical and low-cost labeling advantage. The RFID operating band includes 125/135 kHz (low-frequency band, LF), 13.56 MHz (high-frequency band, HF), 433/860–960 MHz (ultrahigh-frequency band, UHF), and 2.45/5.8 GHz (microwave band, MW). The MW-band RFID system has unique technical superiorities of excellent transmitting rate and distance in a compact configuration for the active RFID technique.

Furthermore, operating at multiple frequencies in compact RFID system has become a critical need to enhance efficiency. Some multiband (FCC UHF and MW bands) linear polarization (LP) solutions have been proposed in [1–4]. A pair of interlaced triangles has been embedded as a star slot in the center of the delta-shaped planar antenna to achieve multiband operation [1]. In [2], a dual-layer configuration with a hexagonal ring patch has been introduced. Finally, an aperture-fed and a marquise-brilliant-diamond-shaped (MBDS) structure are designed in [3, 4].

Compared with LP antenna, CP antenna is more proper for RFID application due to its superiorities, such as detecting insensitivity of the physical orientations and reduced multipath fading. Some dual-band CP designs have been proposed, and most of them employed corner-truncated stack-up configurations [5–7] or slot-coupling structures [8, 9]. In [10], a pair of concentric ring antenna elements are activated with apertures for CP radiation and occupies the whole area of $0.5\lambda \times 0.5\lambda$. However, these single-feed solutions' bandwidths are pretty narrow. Dual-band CP antennas with isolated ports are proposed in [11–16]. In [11–13], traditional phase-delay feeding networks and multiple radiation elements are employed for broad bandwidth and high port isolation. Two corner-chamfered patches and three substrates are stacked in [14] to achieve compact size. However, its axial ratio (AR) bandwidth in the higher band (7 GHz) is narrow (0.1 GHz). In [15], four inverted-F antennas (IFAs) and a 90° phase-delay feeding network are implemented for the FCC UHF-RFID

band. A corner-truncated patch has been printed in the center of the IFAs for the second WLAN band. This solution has a compact volume of $0.5 \times 0.5 \times 0.05\ \lambda^3$, but the maximum realized gains are low (−0.6 and 1.2 dBic) during its FCC RFID and WLAN bands. A dual-band CP RFID solution with separate Tx and Rx ports has been introduced with a dual-band metamaterial branch-line coupler [16]. Every port in its structure operates for both bands, leading to low isolation of 10 dB.

Recently, RFID research focuses on multiple radiating elements in the reader and tag. Compared with the single-input-single-output (SISO) RFID system, the MIMO RFID system greatly enlarges the cover area, solves the non-line-of-sight (NLoS) problem, and obtains better data transmission and information-carrying capacity. Multiradiation-element has been firstly used for RFID systems in [17]. In [18], the SISO RFID and MIMO RFID channel's multipath fading are compared, and the MIMO RFID technique can effectively enhance the fading depth. A distributed antenna system (DAS) for RFID is proposed to compare with a single-antenna RFID system [19]. When the DAS RFID system works in a $10\,m^2$ space, it can obtain a successful reading rate of 100%. In comparison, the conventional SISO RFID system's reading rate is lower than 60%. In [20], a 2×2 MIMO frontend for the RFID MIMO system verifies the RFID MIMO system's superiority of beamforming, diversity combining, and localization at the RFID reader.

So far, some relevant dual-band CP antennas or single-band CP MIMO antennas for RFID applications have been proposed [21, 22]. However, the dual-band CP MIMO solutions with independent-frequency ports for RFID systems are rare. Reference [23] duplicates its dual-feed dual-band CP RFID antenna elements for the 2×2 MIMO system and implements decoupling structures to enhance its port isolation. However, this solution significantly enlarged the overall dimensions and design complexity.

This paper introduces a dual-band CP MIMO antenna for FCC UHF (0.902–0.928 GHz) and MW-RFID (2.4–2.485) system. The four-port configuration, consisting of four inverted-F monopoles fed with a 90° phase-delay feeding network and a corner-truncated patch fed with a square ring slot, can apply to 2×2 MIMO system without dimension increase. The novel contributions of the solution are summarized as follows:

(i) MW-RFID systems that work at 2.45 GHz have many superiorities, such as excellent reading range and speed and ample information storage. Nevertheless, the MW-RFID antenna's design is more complex. Kinds of MW-RFID solutions have been introduced in [24–26]. However, all of them are designed for linear polarization (LP) with a single feed and cannot work at the second FCC UHF-RFID band. Since these two standards (0.915/2.45 GHz) need to operate simultaneously in one system, the four-feed dual-band antenna in this paper is necessary. Furthermore, compared to LP antennas in the RFID systems, the CP antenna has other advantages of decreased multipath fading and adaptability to extreme climatic conditions.

(ii) Traditional CP antennas with dual ports to transmit and receive simultaneously need complex and separated feeding networks for their multiple ports [27–29]. In this paper, a novel dual-port shared phase-delay feeding network, which consists of only two 90° hybrid couplers, has been proposed for the FCC UHF band. It can simultaneously achieve orthogonal-CP radiation fields to enhance port isolation in a more compact dimension. Moreover, most dual-band CP radiating elements need to duplicate their structure to realize MIMO function. This solution with two pairs of independent-band ports can directly apply for MIMO systems without any dimension increase.

(iii) Multifrequency antennas operating at FCC UHF/MW-RFID bands are essential for RFID systems. The MW-RFID reader can transmit collected data to a data processor with a wireless local area network (WLAN). Moreover, multifeed solutions can work as a receiving (RX) and transmitting (TX) antenna simultaneously and further apply to the Bluetooth and Wi-Fi application in industrial, scientific, and medical (ISM) bands.

The antenna design process is elucidated in Section 2, and its simulated and measured results are compared in Section 3. The antenna's application for the MIMO system is discussed in Section 4. Conclusions are proposed in Section 5.

2. Antenna Design

Figure 1 shows the stack-up configuration's layout that includes three 1.53 mm-thickness substrates. Layers 1 and 2 adopt FR 4 ($\varepsilon_r = 4.3$, $\tan\delta = 0.025$) substrate due to its good permittivity and cost performance. Since the feeding network has a critical need for low electromagnetic loss, Rogers Ro4350b ($\varepsilon_r = 3.48$, $\tan\delta = 0.0037$) is suitable as the feeding network's substrate (Layer 3). Two feed lines and the radiating patch for the 2.45 GHz MW-RFID band are printed on the bottom side of Layers 2 and 1, respectively. A 90° phase-delay feeding network has been printed on Layer 3 to feed the four IFA elements for the CP field in the 0.915 GHz UHF-RFID band. All the inverted-F monopoles are on the top side of Layer 1.

2.1. FCC UHF-RFID (0.915 GHz) Feeding and Radiating Configuration. The CP field at the FCC UHF-RFID band has been realized through four inverted-F monopoles and a 90° phase-delay feeding network [16]. Four inverted-F monopoles are printed on Layer 1 top side with 90° clockwise rotation. The meandered monopoles have been employed to decrease the mutual interference with a compact size. Thus, the actual monopole length d_2 reduces from 72 mm to 51 mm.

Since the feeding network needs low electromagnetic loss, this solution adopts Rogers Ro4350b ($\varepsilon_r = 3.48$,

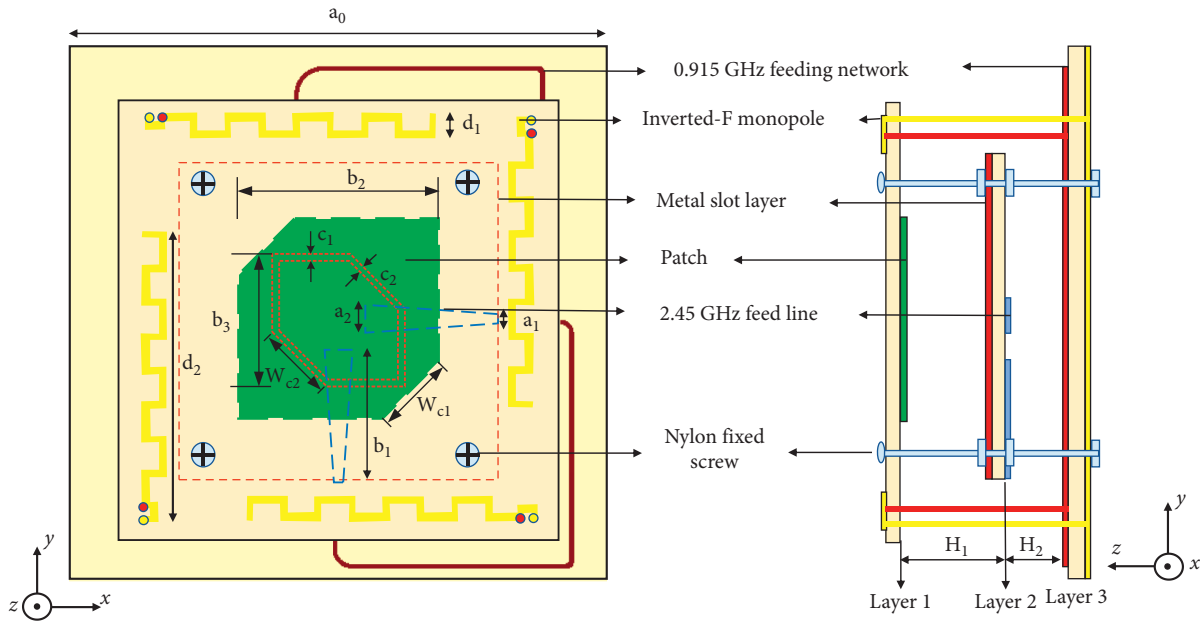

Figure 1: Antenna structure's top view and side view.

tan$\delta = 0.0037$) as Layer 3's dielectric substrate. The phase-delay feeding network with four outputs has been printed on Layer 3's top surface. The inherent four-section branch lines with Z_c and Z_d impedance values are utilized to form a conventional 90° hybrid coupler. Four groups of different-width (W_4 and W_5) branch lines with impedance values of Z_a and Z_b are proposed to achieve dual-band impedance transformers from source impedance to load impedance. Since the different-width impedance transformer's resonate frequencies are set close, a wide impedance bandwidth of the feeding network is realized. It should be noted that the four groups of branch lines are with the same electrical length ($\theta = 90°$).

Moreover, the 90° hybrid couplers' input impedances are 100 Ω because of the parallel relation of the two couplers. The output impedances of Ports 3–6 are 50 Ω and can connect with standard radiating elements directly.

As shown in Figure 2, the inner and outer conductors of the coaxial line have been connected with the two input points of the ports, respectively. Thus, dual-way signals with the same amplitude as well as 180° phase difference have been transmitted to two 90° hybrid couplers. Each of the four outputs obtains a successive 90° phase offset to enhance CP purity. As confirmed by Figure 3, left-hand circular polarization (LHCP) and right-hand circular polarization (RHCP) have been realized with 90° phase progression in Ports 1 and 2, respectively. The orthogonal-CP mode can further enhance the port isolation in the FCC UHF band.

Four groups of pin headers are used to connect the feeding network and four inverted-F monopoles. Each group includes two pairs of pin headers. One pair of pin headers are used as a feed line (connects the monopole and the feeding network) and shorting line (connects the monopole and the ground plane), respectively. Another pair of isolated fixed pin headers has been employed for structure stabilization.

Figure 4 presents the S-parameters of the initial feeding network. The impedance bandwidth covers the entire 0.915 GHz band with the isolation of 20 dB, confirming the initial feeding network solution's feasibility.

2.2. MW-RFID (2.45 GHz) Feeding and Radiating Configuration. The aperture coupling technique introduced by Pozar has some advantages such as shielding the antenna from feeding-network spurious radiation and broad bandwidth [30, 31]. Typically, square slots excited by microstrip lines are used to feed a printed patch antenna electromagnetically. Because the slot interrupts the longitudinal current flow, the coupling of the slot to the patch and the microstrip line's dominant mode occurs. The ring slot structures have been introduced to feed the microstrip patch antenna [32–35]. Two-port linearly polarized patch antennas, especially, excited by a square ring slot are proposed in [32, 33]. Four dual-port linearly polarized aperture-coupled antennas are combined with a sequential rotation feeding technique to achieve an excellent polarization purity CP radiation field [34]. Moreover, a single-feed CP aperture-coupled square ring slot microstrip antenna has been proposed in [35]. The CP radiation field is realized with only one port by introducing a slight asymmetry in the square ring and patch geometries.

In this paper, the proposed solution includes a dual-port dual-CP aperture-coupled microstrip patch excited by a ring slot. Different from [35], two orthogonal CP fields can be achieved by the same aperture-shared dual-port radiating element at 2.45 GHz RFID band without using bulky matching and phase-delay networks.

As in ring-slot-coupling feeding techniques, the ringside length b_3 has been set close to $\lambda/4$. Two orthogonal microstrip feeding lines are employed at two consecutive

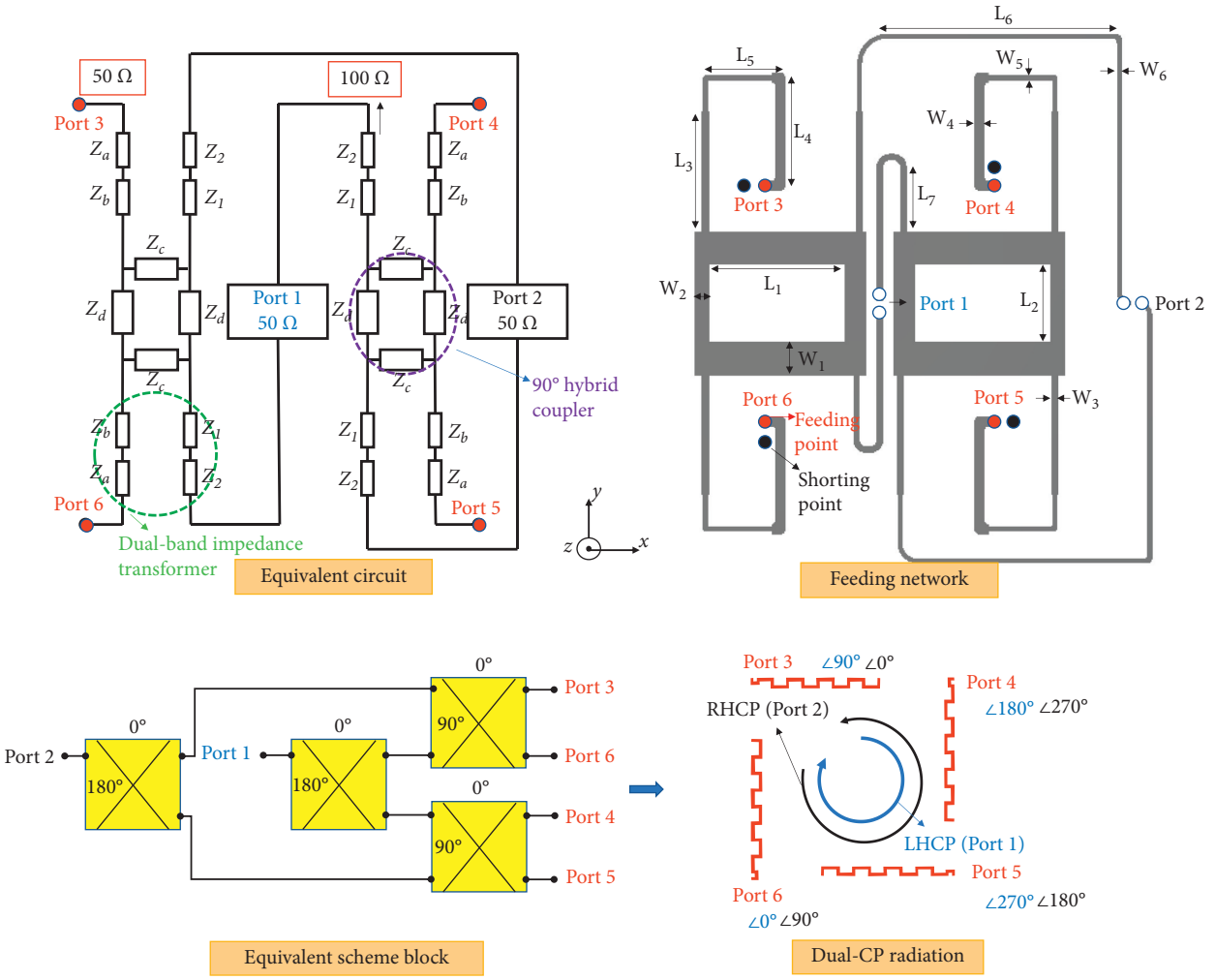

Figure 2: 90° phase-delay feeding network.

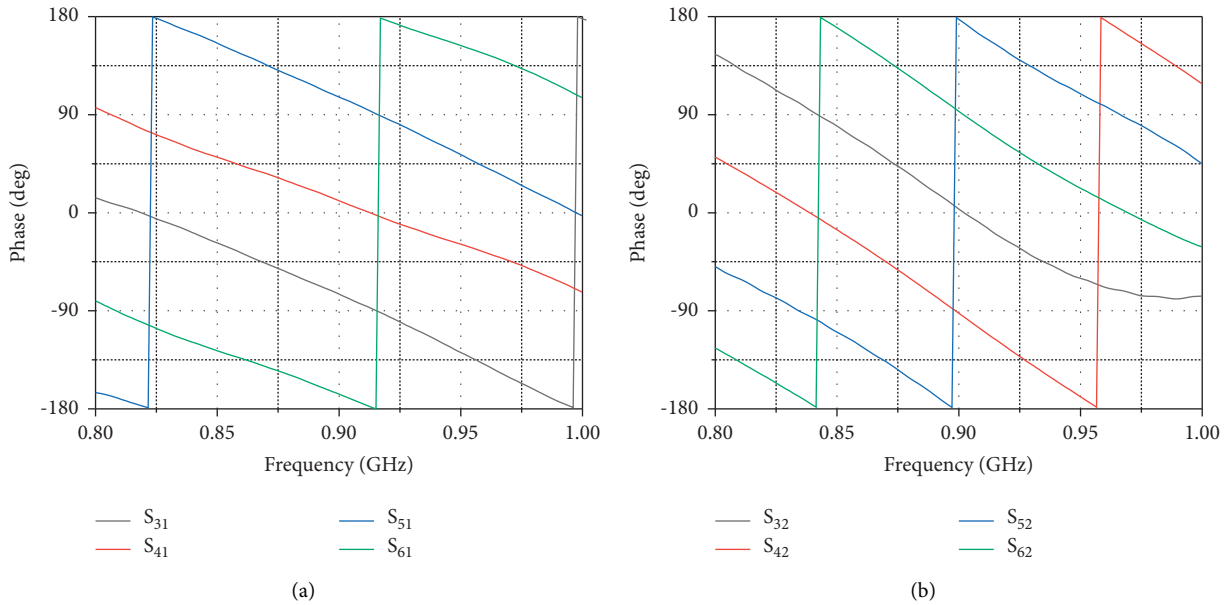

Figure 3: Phase progression in (a) Port 1 to make up LHCP signal and (b) Port 2 to make up RHCP signal.

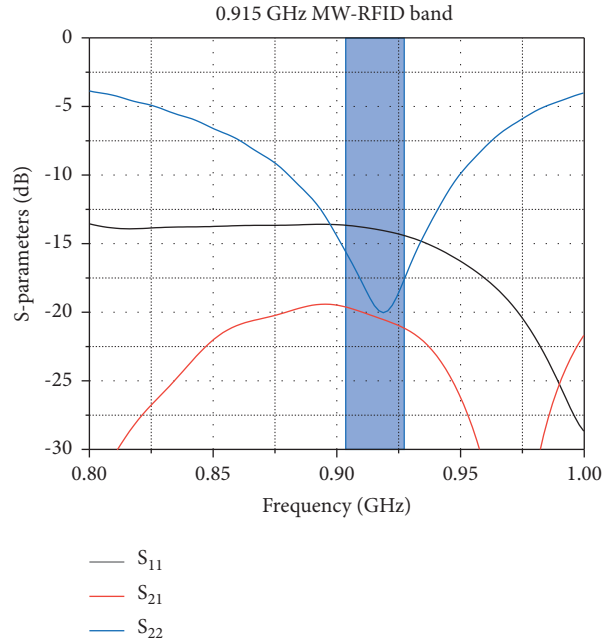

Figure 4: S-parameters of the feeding network for FCC UHF-RFID band.

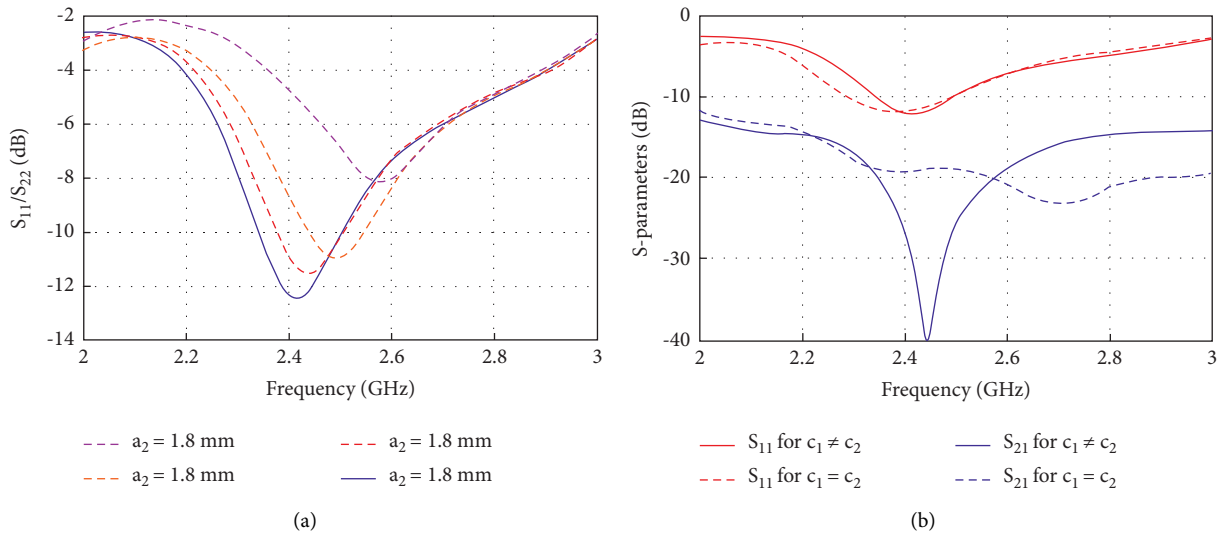

Figure 5: S-parameters comparison of (a) using different stub width a_2 and (b) employing nonuniform-width slot.

edges. A printed patch was then printed at a distance H_1. Its side b_2 is a little different from $\lambda/2$ to obtain a slightly different resonant frequency. The H_1 is parametrically optimized together with the patch size to achieve resonance at the 2.45 GHz RFID band.

Hence, an asymmetry has been introduced in both the ring slot and patch geometries to generate the CP field. Some different perturbations are proposed in the literature to excite the two orthogonal fundamental modes of a patch antenna. In this regard, it is worth mentioning that the diagonal fed a nearly square patch, the corner-truncated patch, and the square patch with peripheral cuts or tuning stub [36]. In this solution, two opposite corners of both the ring slot and resonant patch have been chamfered to obtain a corner-truncated configuration. The ground plane of 0.915 GHz feeding network from Layer 3 bottom can act as the metal reflector of 2.45 GHz radiating structure to reduce its backradiation and increase its gain.

Employing the tapered-width feed line and nonuniform-width slot can further enhance the antenna's S-parameter performance [37]. In Figure 5(a), as the increasing of stub terminal width a_2, the antenna achieves a better impedance matching. The S_{11}/S_{22} decreases from −8 to −12 dB. In Figure 5(b), thanks to the nonuniform-width slot structure,

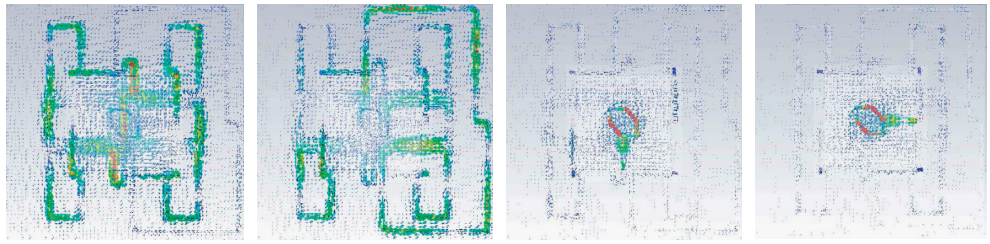

Figure 6: Surface current at Ports 1–4 modes: (a) Port 1 mode, 0.915 GHz, (b) Port 2 mode, 0.915 GHz, (c) Port 3 mode, 2.45 GHz, and (d) Port 4 mode, 2.45 GHz.

the S_{21} decreases from 18 dB to 27 dB in the MW-RFID band. At the same time, the S_{11} keeps stable and is lower than −10 dB.

The surface current distribution when Ports 1–4 are excited has been proposed. As shown in Figure 6, the surface currents focus on the feeding network and four meandered monopoles at Ports 1 and 2 modes. At Ports 3 and 4 modes, the surface currents focus on the tapered-width stub and the ring slot. Thus, a low coupling level between Ports 1 and 2 and Ports 3 and 4 has been realized. The structure parameters have been optimized and listed in Table 1.

Table 1: Structure parameters.

Parameter	Value (mm)
a_0	200
a_1	1.8
a_2	11.7
b_1	38.4
b_2	37
b_3	28.4
c_1	0.89
c_2	0.71
d_1	3
d_2	51
W_1	14.6
W_2	6.7
W_3	3.2
W_4	4.6
W_5	2.1
W_6	2
W_{c1}	16.4
W_{c2}	17.4
L_1	59.3
L_2	34.1
L_3	52.7
L_4	40.1
L_5	29.1
L_6	100.5
L_7	28.3
H_1	13.8
H_2	9.3

3. Antenna Performance and Discussion

The proposed antenna has been prototyped and measured. Its figures of two FR 4 substrates and one Rogers Ro4350b substrate are shown in Figure 7. As shown in Figure 8, the numerical and experimental S-parameters demonstrate a good agreement. The measured −10 dB bandwidths are in the range of 0.875–0.975 GHz (10.9%) and 2.37–2.6 GHz (9.4%), which cover the entire FCC UHF/MW-RFID operating band (0.902–0.928 and 2.4–2.485). As shown in Figure 9, all different-band port isolations ($|S_{31}|$, $|S_{41}|$, $|S_{32}|$, and $|S_{42}|$) are higher than 25 dB because of the proper distance between the corner-truncated patch and inverted-F monopoles. In addition, both the monopole element (working at 0.915 GHz) and slot-coupling element (working at 2.45 GHz) are single frequency radiating configurations without broad bandwidth, and their electrical sizes have a noticeable difference for their different resonate frequencies. Thus, sound isolations have been realized between the antenna elements without any decoupling structures. However, due to the slight reflection in the connection position between the pin headers and the radiation monopoles, there is little same-band port isolation ($|S_{21}|$) deterioration during the FCC UHF band in Figure 9(a). Thus, the 20 dB isolations are obtained among all required bands.

In the center of Figure 10, the proposed fabrication has been measured in the anechoic chamber. The measured radiation patterns are compared with simulated results in the *XZ* and *YZ* planes at 0.915 and 2.45 GHz. The proposed antenna realizes LHCP when Ports 1 and 3 are excited, and the cross-polarizations (RHCP) are better than −20 dB and −18 dB around the broadside (*z*-axis) at Ports 1 and 3, respectively. RHCP is realized when Ports 2 and 4 are excited, and the cross-polarizations (LHCP) at Ports 2 and 4 are lower than −20 dB and −17 dB around the broadside, respectively. The half-power bandwidths (HPBW) are about 75° at 0.915 GHz (Ports 1 and 2) and 50°at 2.45 GHz for broadside cases in *XZ* and *YZ* planes. The maximum measured realized gains in the broadside direction are 4.1 dBic in 0.915 FCC UHF-RFID band for Ports 1 and 2, and 7.2 dBic in 2.45 GHz MW-RFID band for both Ports 3 and 4.

The axial ratio (AR) for broadside cases has been measured with a 20 MHz frequency step. As shown in Figure 11, the numerical and experimental AR exhibits a reasonable agreement. The measured 3-dB ARBWs are 0.83–0.96 GHz (14.2%) and 2.37–2.55 GHz (7.4%), covering the required UHF/MW-RFID bands.

The results of both the measured and simulated AR variations versus the θ-angle are shown in Figures 12 and 13. In the 0.915 GHz UHF-RFID band, the measured 3-dB AR

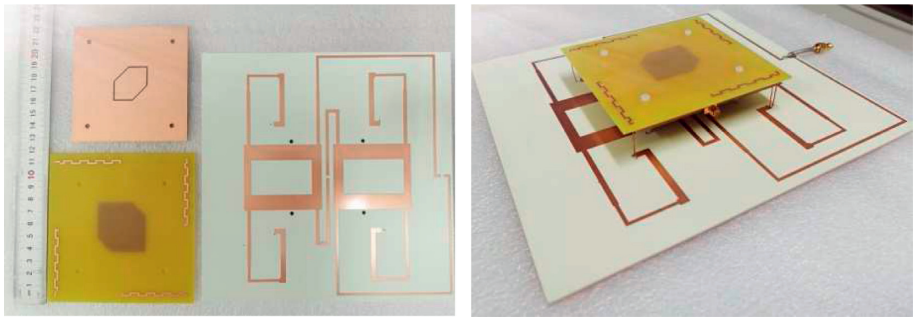

Figure 7: Antenna prototype.

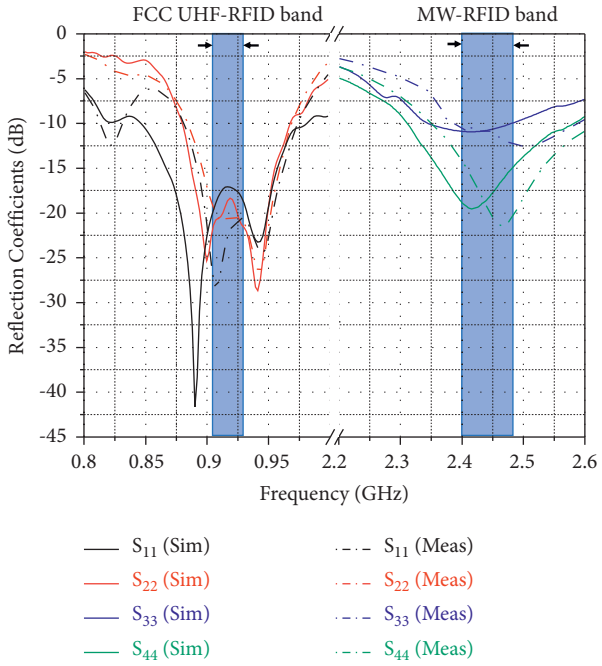

Figure 8: Simulated and measured reflection coefficients of the antenna.

beam widths are 60° and 45° at Port 1 mode and Port 2 mode, respectively. The cross-polar level is slightly higher during the 2.45 GHz band with clear peaks around $\theta = \pm 60°$, especially in Port 4. The measured 3-dB AR beam widths are 44° at Port 3 mode and 30° at Port 4 mode because of surface-wave diffraction at the edges of the dielectric slab [13]. The diffraction from the dielectric layer's edges also occurs in the lower band but is less severe due to the small dielectric layer's relative thickness. If the configuration is designed in a more extensive laminate, the surface waves' effect will reduce. Thus, a trade-off between the antenna miniaturization and the achievable AR beam width has been considered to guarantee an acceptable RFID tag reading coverage. Furthermore, the electromagnetic band-gap (EBG) technique can also decrease the effect of diffraction [38].

4. Application for MIMO System

The ECC and DG are the MIMO system's critical performance index. In consideration of the antenna's spatial influence, the ECC can be estimated from the far-field radiation pattern by the following [39]:

$$\rho_e = \left| \frac{\iint_{4\pi} \left[\overrightarrow{E_1}(\theta,\phi) \cdot \overrightarrow{E_2}(\theta,\phi) \right] d\Omega \Big|^2}{\iint_{4\pi} \left| \overrightarrow{E_1}(\theta,\phi) \right|^2 d\Omega \iint_{4\pi} \left| \overrightarrow{E_2}(\theta,\phi) \right|^2 d\Omega}, \right. \tag{1}$$

$$\mathrm{DG} = 10\sqrt{1 - \left(0.99\rho_e\right)^2} \tag{2}$$

The calculated ECC and DG are proposed in Figure 14. The ECC during the requiring band meets the criterion of

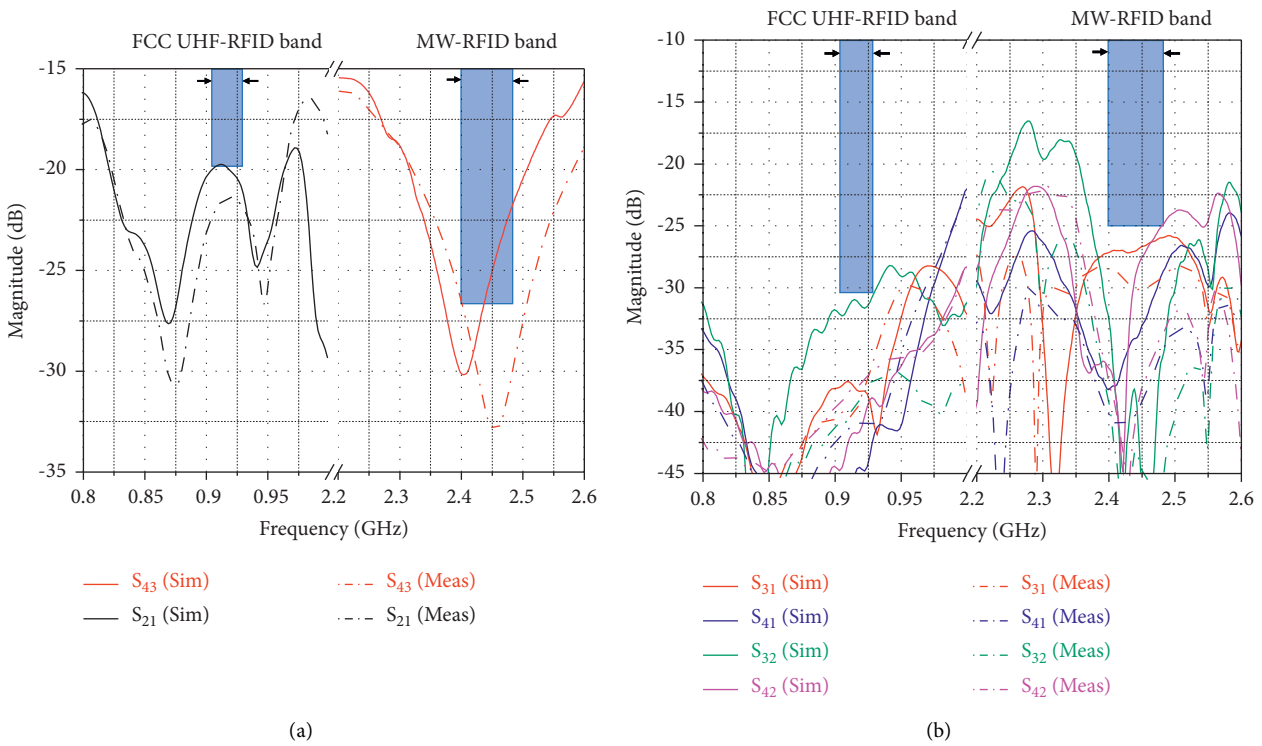

Figure 9: Simulated and measured isolation of (a) same-band ports and (b) different-band ports.

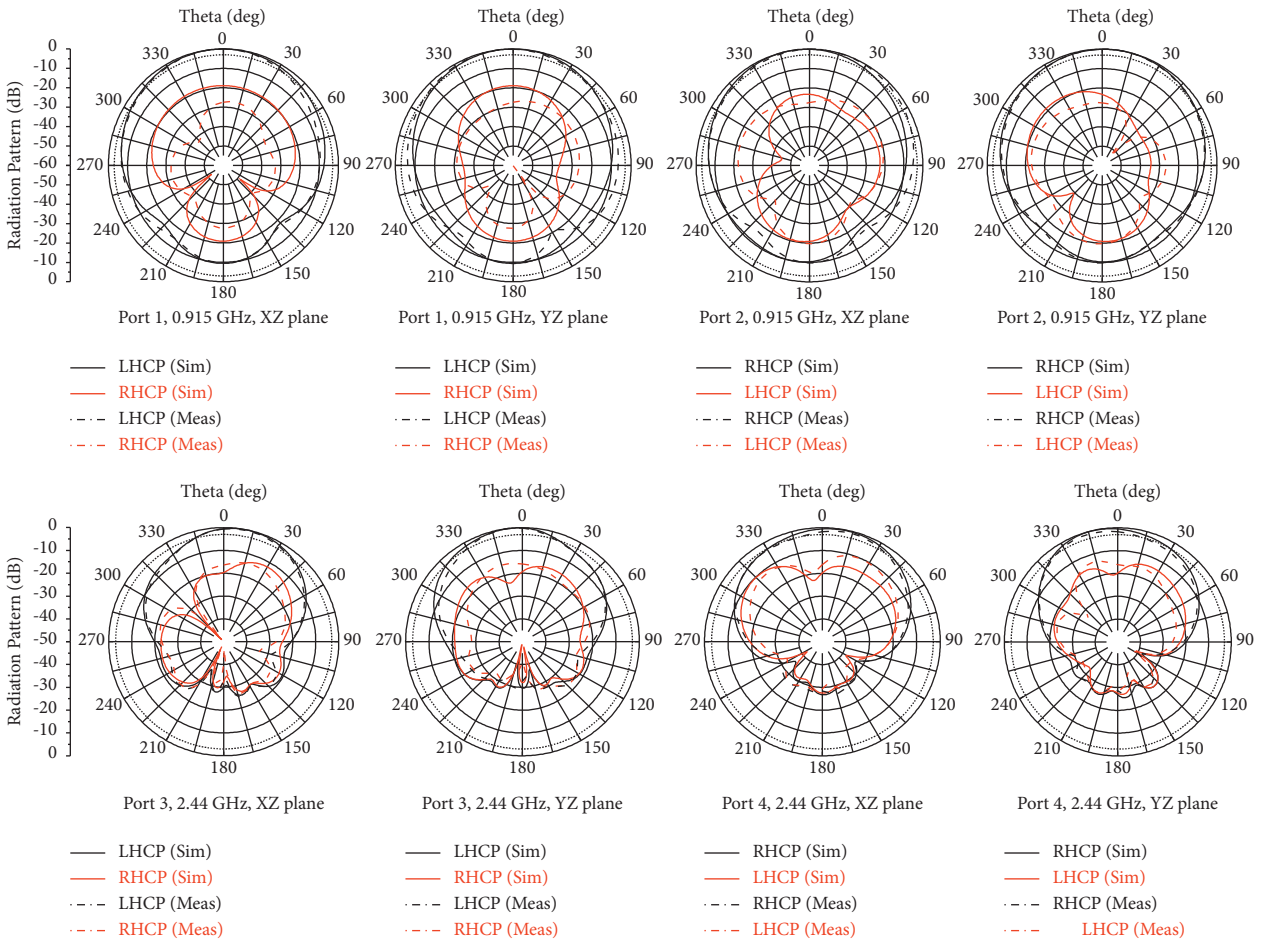

Figure 10: Simulated and measured normalized radiation patterns at Ports 1 and 2 (0.915 GHz) and Ports 3 and 4 (2.44 GHz) in *XZ* and *YZ* planes.

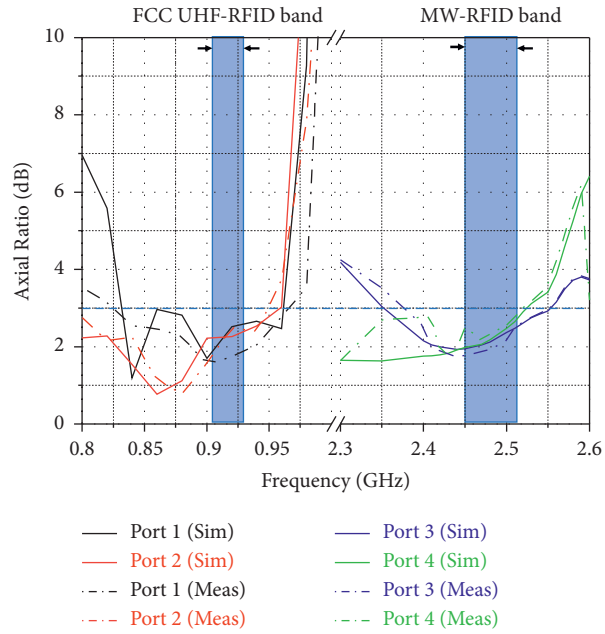

Figure 11: Simulated and measured axial ratio.

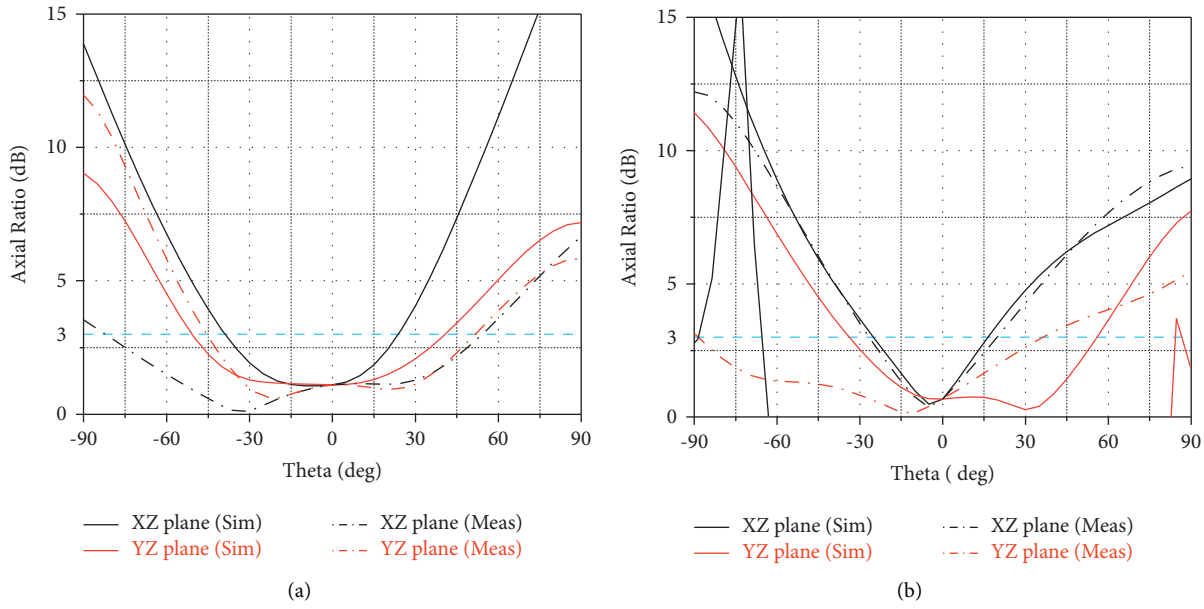

Figure 12: Simulated and measured axial ratio as a function of θ angle from the broadside, in the XZ and YZ planes at 0.915 GHz: (a) Port 1 and (b) Port 2.

0.01 [37], which means that similar channel capacities are realized for both spatial and polarization diversity. Thus, the proposed antenna can be employed for MIMO application with polarization diversity of both same-band ports (Ports 1 and 2 in UHF band and Ports 3 and 4 in MW band). The DG gets closer to its theoretical maximum value of 10 dB and ensures good MIMO performance.

Table 2 compares the proposed solution with other relevant dual-band CP antenna solutions. Compared with dual-band CP RFID solutions ([9, 10, 15, 16]), this solution has a more balanced and excellent performance. Moreover, most dual-band CP solutions need to duplicate their structures for MIMO applications, significantly increasing their whole dimensions. Considering MIMO application, [21, 22] are the multiband CP MIMO antennas, but each port in their solutions needs to work for multiple operating bands. Notably, the dual-band antennas working simultaneously with separated single-band ports (each port work in

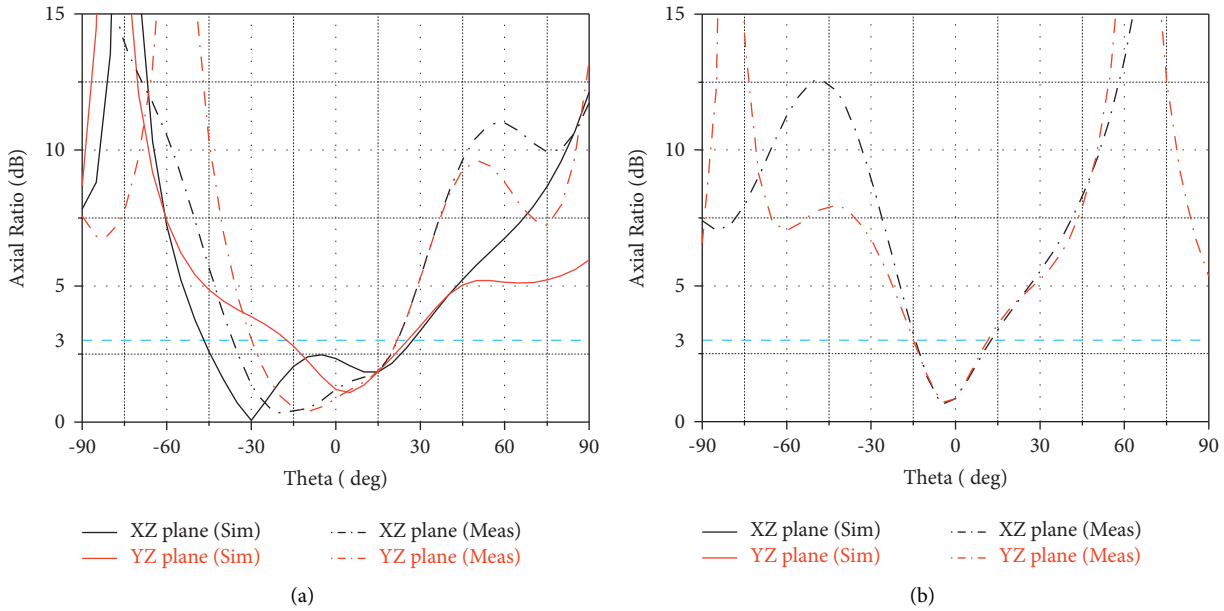

Figure 13: Simulated and measured axial ratio as a function of θ angle from the broadside, in the XZ and YZ planes at 2.45 GHz: (a) Port 3 and (b) Port 4.

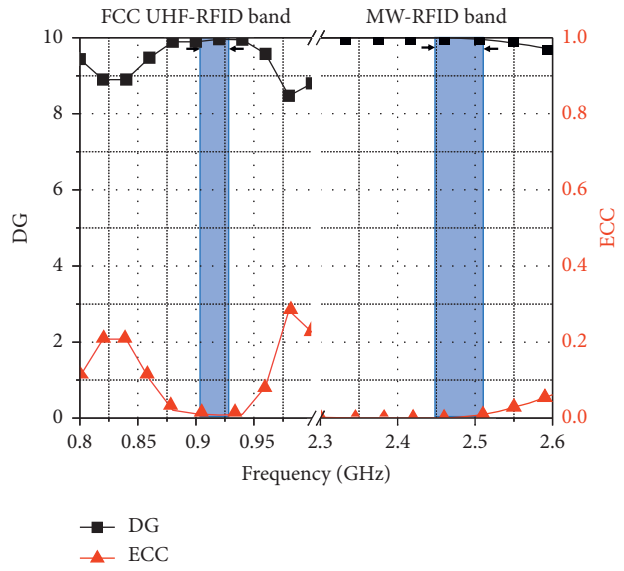

Figure 14: Calculated ECC and DG.

Table 2: Performance comparison with other proposed dual-band multiport CP antenna systems.

Ref.	Size [λ^3]	Ports and polarization	Bands (GHz)	IBW (%)	ARBW (%)	Isolation (dB)	Gain [dBic]	ECC
[9]	$0.6 \times 0.6 \times 0.09$	One port	0.915	2.6	5.3	—	2.9	—
		Same sense	2.45	2	2		6.1	
[10]	$0.5 \times 0.5 \times 0.04$	One port	0.92	4.8	4.8	—	6.5	—
		Dual-sense	2.45	16.7	16.7		7	
[15]	$0.6 \times 0.6 \times 0.05$	Two ports	0.915	2.8	2.8	25	−0.6	—
		Same sense	2.45	3.2	0.8	20	1.2	
[16]	$0.7 \times 0.7 \times 0.1$	Two ports	0.92	3.4	4.4	10	6.6	—
		Dual-sense	2.45	7	8.2	10	7.9	

Table 2: Continued.

Ref.	Size [λ^3]	Ports and polarization	Bands (GHz)	IBW (%)	ARBW (%)	Isolation (dB)	Gain [dBic]	ECC
[21]*	$0.9 \times 0.6 \times 0.01$	Two ports	2.45	20	—	20		
		Dual-sense	3.5	18.8	5	16	—	0.5
			5.3	15.2	—	18		
[22]	$0.8 \times 0.2 \times 0.01$	Two ports	2.45	36	36	15	6	0.0001
		Dual-sense	5.8	17	17	20	2.6	0.0001
[23]	$1.1 \times 0.5 \times 0.11$	Four ports	2.45	12.7	3.5	25	7.3	0.03
		Dual-sense	5.8	5.1	6.2	30	7.3	0.03
This work	**$0.6 \times 0.6 \times 0.07$**	**Four ports**	**0.915**	**10.9**	**14.2**	**20**	**4.1**	**0.01**
		Dual-sense	**2.45**	**9.4**	**7.4**	**25**	**7.4**	**0.01**

*The radiating elements radiate two orthogonal LP fields at the WLAN band and CP field in the range 3.31–3.48 GHz (within the WiMAX band). Antenna performance here indicated refers to the WiMAX band, where a CP MIMO system is obtained.

only one required band) are always necessary for the MIMO system [23]. The solution in this paper achieves dual-band CP simultaneous operation with two pairs of single-band ports and occupies a more compact dimension. Thus, the proposed solution is better for the dual-band RFID 2×2 MIMO system compared with other solutions.

5. Conclusions

A compact, four-port, dual-band, dual-CP antenna for UHF/MW-RFID MIMO systems has been introduced, prototyped, and characterized. Shared-aperture and non-uniform-width slot has been designed for the MW-RFID band to increase the isolation and impedance matching. Thanks to the four inverted-F meandered monopoles and phase-delay feeding network, the antenna can obtain the second FCC UHF-RFID working band with a compact overall dimension. The measured antenna performance of S-parameters, AR, radiation pattern, and realized gain agree with the simulated results. Good ECC and DG performance demonstrate that the proposed solution is suitable for dual-band CP RFID MIMO applications.

Data Availability

The data used to support the findings of this study are available from the corresponding author upon request.

Conflicts of Interest

The authors declare that there are no conflicts of interest regarding the publication of this paper.

Acknowledgments

This work was funded in part by the National Natural Science Foundation of China (grant nos. 61731007 and U1633202).

References

[1] M. M. A. El-Negm Yousef and A. B. Abdel-Rahman, "Realization of multi-band antenna for WiMAX and RFID by etching two interlaced triangles from delta resonator," in *Proceedings of 2017 34th National Radio Science Conference (NRSC)*, pp. 79–86, Alexandria, Egypt, March 2017.

[2] C. Bajaj, D. K. Upadhyay, S. Kumar, and B. K. Kanaujia, "Compact dual-band hexagonal ring antenna with shorting pins for RFID reader applications," in *Proceedings of 2020 7th International Conference on Signal Processing and Integrated Networks (SPIN)*, pp. 405–408, Delhi, India, February 2020.

[3] F. Y. Kuo, P. H. Pan, C.-Y. Chiang, H. T. Hsu, and H. T. Chou, "Dual band aperture-coupled patch antenna for RFID mobile terminal applications," in *Proceeding of Asia-Pacific Microwave Conference (APMC)*, pp. 2201–2204, Yokohama, Japan, December 2010.

[4] M. I. Sabran, S. K. A. Rahim, A. Y. A. Rahman, T. A. Rahman, and M. Z. M. Nor Evizal, "A dual-band diamond-shaped antenna for RFID application," *IEEE Antennas and Wireless Propagation Letters*, vol. 10, pp. 979–982, 2011.

[5] B. Huang, Y. Yao, and Z. Feng, "A novel wide beam dual-band dual-polarization stacked microstrip-dielectric antenna," in *Proceedings of the 2007 International Conference on Microwave and Millimeter Wave Technology*, pp. 1–4, Guilin, China, 2007.

[6] X. Sun, Z. Zhang, and Z. Feng, "Dual-band circularly polarized stacked annular-ring patch antenna for GPS application," *IEEE Antennas and Wireless Propagation Letters*, vol. 10, pp. 49–52, 2011.

[7] R. K. Vishwakarma, "Design of rectangular stacked microstrip antenna for Dual-band," in *Proceedings of International Conference on Emerging Trends and Photonic Devices & Systems*, pp. 22–24, Varanasi, India, December 2009.

[8] X.-B. Sun, "Circular-slotted microstrip antenna for GPS," *Microwave and Optical Technology Letters*, vol. 52, no. 5, pp. 999-1000, 2010.

[9] S. Sarkar and B. Gupta, "A dual-band circularly polarized antenna with a dual-band AMC reflector for RFID readers," *IEEE Antennas and Wireless Propagation Letters*, vol. 19, no. 5, pp. 796–800, 2020.

[10] H. T. Hsu and T. J. Huang, "Aperture-coupled dual-band circularly polarized antenna for RFID reader applications," in *Proceedings of Cross Strait Quad-Regional Radio Science Wireless Technology Conference. (CSQRWC)*, pp. 52–55, Taipei, Taiwan, July 2012.

[11] J. Ha, M. A. Elmansouri, P. Valale Prasannakumar, and D. S. Filipovic, "Monostatic Co-polarized full-duplex antenna with left- or right-hand circular polarization," *IEEE Transactions on Antennas and Propagation*, vol. 65, no. 10, pp. 5103–5111, 2017.

[12] C.-X. Mao, Z. H. Jiang, D. H. Werner, S. S. Gao, and W. Hong, "Compact self-diplexing dual-band dual-sense circularly polarized array antenna with closely spaced operating

frequencies," *IEEE Transactions on Antennas and Propagation*, vol. 67, no. 7, pp. 4617–4625, 2019.

[13] A. B. Smolders, R. M. C. Mestrom, A. C. F. Reniers, and M. Geurts, "A shared aperture dual-frequency circularly polarized microstrip array antenna," *IEEE Antennas and Wireless Propagation Letters*, vol. 12, pp. 120–123, 2013.

[14] L. S. Pereira and M. V. T. Heckler, "Dual-band dual-polarized microstrip antenna for Rx/Tx terminals for high altitude platforms," in *Proceedings of 2015 9th European Conference on Antennas and Propagation (EuCAP)*, pp. 1–5, Lisbon, Portugal, April 2015.

[15] R. Caso, A. Michel, M. Rodriguez-Pino, and P. Nepa, "Dual-band UHF-RFID/WLAN circularly polarized antenna for portable RFID readers," *IEEE Transactions on Antennas and Propagation*, vol. 62, no. 5, pp. 2822–2826, May 2014.

[16] Y.-K. Jung and B. Lee, "Dual-band circularly polarized microstrip RFID reader antenna using metamaterial branch-line coupler," *IEEE Transactions on Antennas and Propagation*, vol. 60, no. 2, pp. 786–791, 2012.

[17] J. D. Griffin and G. D. Durgin, "Gains for RF tags using multiple antennas," *IEEE Transactions on Antennas and Propagation*, vol. 56, no. 2, pp. 563–570, 2008.

[18] J. D. Griffin and G. D. Durgin, "Multipath fading measurements for multi-antenna backscatter RFID at 5.8 GHz," in *Proceedings of 2009 IEEE International Conference on RFID*, pp. 322–329, Orlando, FL, USA, April 2009.

[19] S. Sabesan, M. Crisp, R. V. Penty, and I. H. White, "An error free passive UHF RFID system using a new form of wireless signal distribution," in *Proceedings of 2012 IEEE International Conference on RFID*, pp. 58–65, Orlando, FL, USA, April 2012.

[20] R. Langwieser, C. Angerer, and A. L. Scholtz, "A UHF frontend for MIMO applications in RFID," in *Proceedings of IEEE 2010 Radio and Wireless Symposium*, pp. 124–127, New Orleans, FL, USA, January 2010.

[21] N. K. Sahu, G. Das, A. Sharma, and R. K. Gangwar, "Design of a dual-polarized triple-band hybrid MIMO antenna for WLAN/WiMAX applications," in *Proceedings of 2017 IEEE Conference on Antenna Measurements & Applications (CAMA)*, pp. 246–248, Tsukuba, Japan, December 2017.

[22] A. H. Haghparast and G. Dadashzadeh, "A dual band polygon shaped CPW-fed planar monopole antenna with circular polarization and isolation enhancement for MIMO applications," in *Proceedings of 2015 9th European Conference on Antennas and Propagation (EuCAP)*, pp. 1–4, Lisbon, Portugal, April 2015.

[23] E. Zhang, A. Michel, P. Nepa, and J. Qiu, "Compact dual-band circularly polarized stacked patch antenna for microwave-radio-frequency identification multiple-input-multiple-output application," *International Journal of Antennas and Propagation*, vol. 2021, Article ID 9991748, 13 pages, 2021.

[24] D. Ma and W. X. Zhang, "Broadband CPW-fed RFID antenna at 2.45/5.80 GHz," in *Proceedings of 2007 International Workshop on Anti-counterfeiting, Security and Identification (ASID)*, pp. 84–87, Xiamen, China, October 2007.

[25] A. T. Mobashsher, M. T. Islam, and N. Misran, "A novel high-gain dual-band Antenna for RFID reader applications," *IEEE Antennas and Wireless Propagation Letters*, vol. 9, pp. 653–656, 2010.

[26] A. Sharma, I. J. G. Zuazola, and A. Perallos, "Multipurpose near- and far-field switched multiband coil antenna for 915-MHz/2.45/5.8-GHz RFIDs," *IEEE Antennas and Wireless Propagation Letters*, vol. 16, pp. 2562–2565, 2017.

[27] E. A. Etellisi, M. A. Elmansouri, and D. S. Filipovic, "Wideband monostatic Co-polarized Co-channel simultaneous transmit and receive broadside circular array antenna," *IEEE Transactions on Antennas and Propagation*, vol. 67, no. 2, pp. 843–852, 2019.

[28] Z. Zhou, Y. Li, J. Hu, Y. He, Z. Zhang, and P.-Y. Chen, "Monostatic copolarized simultaneous transmit and receive (STAR) antenna by integrated single-layer design," *IEEE Antennas and Wireless Propagation Letters*, vol. 18, no. 3, pp. 472–476, 2019.

[29] E. A. Etellisi, M. A. Elmansouri, and D. Filipovic, "Broadband full-duplex monostatic circular-antenna arrays: circular arrays reaching simultaneous transmit and receive operation," *IEEE Antennas and Propagation Magazine*, vol. 60, no. 5, pp. 62–77, 2018.

[30] D. M. Pozar, "Microstrip antenna aperture-coupled to a microstrip-line," *Electronics Letters*, vol. 21, no. 4, pp. 49-50, 1985.

[31] R. Garg, P. Bhartia, I. J. Bahl, and A. Ittipiboon, *Microstrip Antenna Design Handbook*, Artech House, Boston, MA, USA, chapter 9, 2001.

[32] R. Caso, A. A. Serra, M. Pino, P. Nepa, and G. Manara, "A wideband slot-coupled stacked-patch array for wireless communications," *IEEE Antennas and Wireless Propagation Letters*, vol. 9, pp. 986–989, 2010.

[33] R. Caso, A. Serra, A. Buffi, M. Rodriguez-Pino, P. Nepa, and G. Manara, "Dual-polarised slot-coupled patch antenna excited by a square ring slot," *IET Microwaves, Antennas & Propagation*, vol. 5, no. 5, pp. 605–610, 2011.

[34] R. Caso, A. Buffi, M. Rodriguez Pino, P. Nepa, and G. Manara, "A novel dual-feed slot-coupling feeding technique for circularly polarized patch arrays," *IEEE Antennas and Wireless Propagation Letters*, vol. 9, pp. 183–186, 2010.

[35] A. Buffi, R. Caso, M. R. Pino, P. Nepa, and G. Manara, "Single-feed circularly polarised aperture-coupled square ring slot microstrip antenna," *Electronics Letters*, vol. 46, no. 4, pp. 268-269, 2010.

[36] A. R. Guraliuc, A. Buffi, R. Caso, and P. Nepa, "Axial ratio analysis of single-feed circularly polarized resonant antennas," *Journal of Electromagnetic Waves and Applications*, vol. 28, no. 6, pp. 716–728, 2014.

[37] E. Zhang, A. Michel, M. R. Pino, P. Nepa, and J. Qiu, "A dual circularly polarized patch antenna with high isolation for MIMO WLAN applications," *IEEE Access*, vol. 8, pp. 117833–117840, 2020.

[38] N. Llombart, A. Neto, G. Gerini, and P. de Maagt, "Planar circularly symmetric EBG structures for reducing surface waves in printed antennas," *IEEE Transactions on Antennas and Propagation*, vol. 53, no. 10, pp. 3210–3218, 2005.

[39] U. Ullah, I. B. Mabrouk, S. Koziel, and M. Al-Hasan, "Implementation of spatial/polarization diversity for improved-performance circularly polarized multiple-input-multiple-output ultra-wideband Antenna," *IEEE Access*, vol. 8, pp. 64112–64119, 2020.